Oxygen adsorption on Fe/W(110) and Co/W(110) thin films: Surface magnetic properties

S. Förster, G. Baum, M. Müller, and H. Steidl
Fakultät für Physik, Universität Bielefeld, D-33615 Bielefeld, Germany
(Received 7 June 2002; published 30 October 2002)

The dependence of surface magnetic properties on oxygen coverage of ordered and unordered Fe/W(110) and Co/W(110) films have been studied by the means of spin-polarized metastable deexcitation spectroscopy. A recently developed deconvolution method allows the direct calculation of the surface spin densities effective in the deexcitation process from measured secondary electron spectra. The O_{2p}-derived surface states show exchange splitting due to magnetic coupling which is dependent on surface order and coverage.

DOI: 10.1103/PhysRevB.66.134427 PACS number(s): 75.70.Rf

I. INTRODUCTION

In recent years, numerous investigations of surface properties of clean and adsorbate covered substrates have been carried out by different methods. A distinct surface sensitivity can be achieved in electron emission by the impact of metastable He($2\,^3S$) atoms of thermal energy, a method called metastable deexcitation spectroscopy (MDS) (e.g., Refs. 1,2, for a general overview see Ref. 3). This technique probes predominantly the outermost atomic layer. The spin selective version of MDS uses an electron-spin-polarized He($2\,^3S$) atomic beam (SPMDS).[4,5] Through the spin selectivity in the deexcitation process at the surface, one has an excellent tool for obtaining information on the magnetic properties of the outermost region of the surface and on the influences due to adsorbates. If the deexcitation process is dominated by a two-electron process [resonance ionization (RI) followed by Auger neutralization (AN)] the measured secondary electron spectra represent a convolution of surface-state densities. Here, a deconvolution of experimental data is needed in the analysis.

The studies of oxygen adsorption on Fe and Co thin films have been done by several groups (e.g., Refs. 5–9). Especially, the interplay between oxygen chemisorption on iron and magnetism of the surface has been extensively studied.[10–13] Oxygen is known to chemisorb dissociatively on Fe and Co.[14–16] The interaction with the substrate causes a hybridization of the atomic states involved in the bond. The adsorbate-induced bands couple magnetically via exchange interaction to the substrate leading to an energy splitting of the bands. The exchange splitting of O_{2p}-derived states has been reported to be dependent on the oxygen coverage[10–12] and on the surface order.[17] Recently published deconvoluted SPMDS data of O/Fe/Ag(001) (Refs. 11,17) and O/Fe/MgO(001) (Refs. 12,13,17) provide an opportunity of comparison to our O/Fe/W(110) data.

II. METHOD OF MEASUREMENT

The details of our experimental setup are given elsewhere.[18,19] Here we want to focus only on aspects needed to interpret the obtained data. We use thin films ($\sim$20 Å) of Fe or Co grown epitaxially on a W(110) crystal at room temperature. A subsequent annealing of these films to about 400 K leads to patterns corresponding to well-defined bcc iron (110) and hcp cobalt (0001) surfaces, as is confirmed by means of low-energy electron diffraction. In these films the surface anisotropy causes the easy magnetization axis to lie in plane along the $[1\bar{1}0]$ direction of the substrate. The films were uniformly magnetized in this direction, collinear to the polarization of the incident He($2\,^3S$) beam. To be consistent with most theoretical and experimental works (e.g. Refs. 10,13,20,21), we define the spin-dependent asymmetry A of ejected electrons by

$$A(E)=\frac{1}{P_A}\,\frac{N_p(E)-N_a(E)}{N_p(E)+N_a(E)}, \tag{1}$$

and the total intensity I of ejected electrons by

$$I(E)=N_p(E)+N_a(E), \tag{2}$$

assuming that full single-domain magnetization of the target is preserved. P_A is the degree of polarization of the atomic beam and $N_p(E)$ [$N_a(E)$] denotes the rates of ejected electrons at kinetic energy E with He($2\,^3S$) spin parallel [antiparallel] to the *majority* electron spin which is opposite to the direction of magnetization. Because of the *opposite* polarization of the He^+ $1s$ hole, which is effective in the interaction, a *positive* asymmetry A indicates a dominance of *minority* electrons.

III. MODEL AND DECONVOLUTION

Depending on the work function ϕ of the surface, the deexcitation of metastable helium atoms occurs either by RI with a subsequent AN, or by Auger deexcitation (AD). If the wave function of the $2s$ electron of the He($2\,^3S$) atom overlaps sufficiently with an empty level of the surface, a tunneling into this state will occur (RI) at large distances from the surface ($z_{RI} \geqslant 5$ Å). The resulting positive ion continues towards the surface and subsequently AN takes place ($z_{AN} \approx 2$–3 Å) with an electron from the solid tunneling into the $1s$ hole of the helium ion. The energy released is transferred to another electron which may be ejected from the solid. Without RI taking place, the metastable atoms come close to the surface and AD will then occur as dominant deexcitation process with the emission of the $2s$ electron of helium. RI is suppressed if the excited $2s$ helium level lies below the Fermi level of the surface or if there is an insufficient overlap with empty states due to an adsorbate layer. But here in an

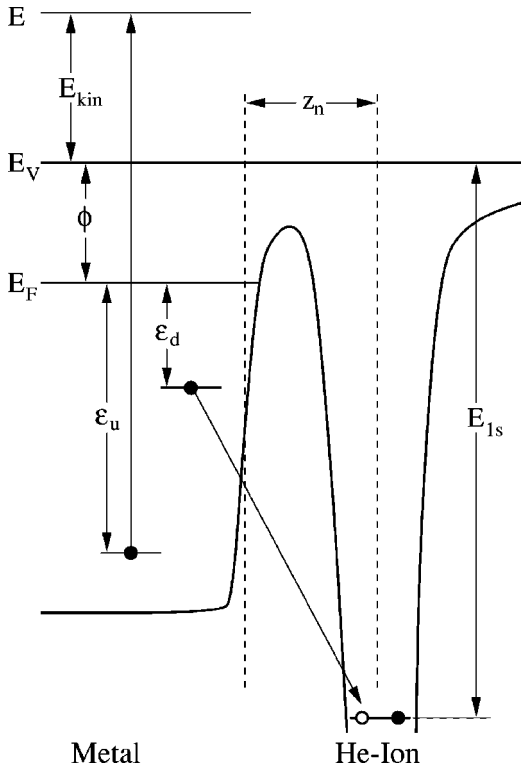

FIG. 1. Auger neutralization of He^+ ion (for details see text).

experimentally accessible binding-energy range (0–10 eV) RI is not suppressed, since the adsorbate O_{2p} states are involved in the bond and accept electrons from the surface.

Theories on MDS and SPMDS (Refs. 20–23) draw the conclusion that the experimental energy distributions $N_a(E)$ and $N_p(E)$ are self-convolutions of the density of states $\rho_\uparrow(\epsilon)$ (majority electrons) and $\rho_\downarrow(\epsilon)$ (minority electrons) *effective* in the AN process. The different arguments E [ϵ] denote different scales of kinetic energy E of the ejected electron and binding energy ϵ of the involved solid-state band electrons. The state density which is effective, here means that the true state densities are weighted by the transition probability. Based on the theory developed by Hagstrum,[22,24] primarily for ion neutralization spectroscopy, the mechanisms taking place are outlined here in brief.

The RI and AN steps in the deexcitation process are effective at well-separated distances from the surface and so can be treated independently. RI is assumed to occur with unit probability, independent of the spin of the incoming helium atom.[20] Therefore the spin-dependent process has to be the Auger neutralization of He^+ ions having a polarized $1s$ hole.

Figure 1 shows schematically the AN process. Given the energy balance $E_{1s}-(\epsilon_d+\phi)=(\epsilon_u+\phi)+E_{kin}$ of the ''down''-tunneling ($_d$) and the ''up''-ejected ($_u$) electron, all electron pairs that hold the relation $\epsilon_d+\epsilon_u=E_{1s}-2\phi-E_{kin}=E_m$ result in an ejected electron with energy E_{kin}.

The intensity distribution $N(E)$ of ejected electrons is therefore given by

$$N(E)\sim\int_0^{E_m}|H_{fi}|^2 n_d(\epsilon)n_u(E_m-\epsilon)d\epsilon, \tag{3}$$

where $n_d(\epsilon)$ is the density of states of the down-tunneling metal electrons at binding energy $\epsilon\equiv\epsilon_d$, $n_u(E_m-\epsilon)$ is the density of the up-emitted electrons, and H_{fi} is the initial to final state transition matrix element of the form

$$H_{fi}=\int\int\chi_{1S}^*(\mathbf{r_2})\psi_V^*(\mathbf{r_1})F(|\mathbf{r_1}-\mathbf{r_2}|)\phi_u(\mathbf{r_1})\phi_d(\mathbf{r_2})d\mathbf{r_1}d\mathbf{r_2} \tag{4}$$

assuming no exchange interaction between the two electrons. Here ϕ_u and ϕ_d are the orbital wave functions of the surface electrons, χ_{1S} is the wave function of the He^+ $1s$ hole, ψ_V is an empty vacuum state, and $F(|\mathbf{r_1}-\mathbf{r_2}|)$ is the screened Coulomb potential between the two involved electrons and $\mathbf{r_1},\mathbf{r_2}$ their position vectors.

To obtain n_u and n_d from $N(E)$ the form of H_{fi} must be known. For this the following simplifying assumptions are made, which are shown to be justified by the results of the deconvolution process e.g., Fig. 6, where the structures seen in ultraviolet photoelectron spectroscopy (UPS) are matched by our deconvolution results:

(i) Neglecting correlation and exchange effects and assuming a constant thickness of the potential barrier between ion and surface ($\int F(|\mathbf{r_1}-\mathbf{r_2}|)d\mathbf{r_1}d\mathbf{r_2}=$const), Eq. (4) can be factorized to

$$H_{fi}\sim\int\chi_{1S}^*(\mathbf{r_2})\phi_d(\mathbf{r_2})d\mathbf{r_2}\int\psi_V^*(\mathbf{r_1})\phi_u(\mathbf{r_1})d\mathbf{r_1}.$$

(ii) Since all final vacuum states ψ_V are open, transition rates for the ''up'' electron depends only on the initial state ϕ_u. The transition rates for the down electron depend on initial state ϕ_d and on the overlap of ϕ_d and χ_{1S} at distance z_n (Fig. 1), where tunneling occurs. z_n is averaged in measurement of $N(E)$.

(iii) Initial states ϕ_u and ϕ_d depend only on initial binding energies of the two electrons. So

$$|H_{fi}|^2\sim|\phi_d(\epsilon)|^2|\phi_u(E_m-\epsilon)|^2. \tag{5}$$

(iv) Assuming a similar orbital symmetry of all participating band electrons originating from the same surface region, ϕ_u and ϕ_d can be set equal, dropping indices in Eq. (5).

(v) So Eq. (3) is transformed into a Laplace convolution integral

$$N(E)=\int_0^{E_m}U_d(\epsilon)U_u(E_m-\epsilon)d\epsilon, \tag{6}$$

introducing the *effective* state densities $U_{u(d)}(\epsilon)=|\phi(\epsilon)|^2 n_{u(d)}(\epsilon)$ or ''transition densities'' probed by $N(E)$.

(vi) $U(\epsilon)$ is the sum of the effective spin densities $\rho_\uparrow(\epsilon)$ (majority) and $\rho_\downarrow(\epsilon)$ (minority). Assuming that up and down electrons originate from the same surface region, $U_u(\epsilon)$ and $U_d(\epsilon)$ can be set equal. Using unpolarized $He(2\,^3S)$ MDS, $N(E)$ so is a self-convolution of $U(\epsilon)$. In SPMDS, because of the polarization of the He^+ $1s$ hole, only an electron with matching spin orientation tunnels. Due to this the density of down electrons U_d is probed spin selectively, revealing the

spin densities $\rho_\uparrow$ and $\rho_\downarrow$. Note that the He^+ $1s$ hole has the *opposite* polarization of the incident He* beam, so that N_p probes $\rho_\downarrow$.

Thus the measured intensities are

$$N(E)_p = \int_0^{E_m} \rho_\downarrow(\epsilon)[\rho_\uparrow(E_m-\epsilon)+\rho_\downarrow(E_m-\epsilon)]d\epsilon,$$

$$N(E)_a = \int_0^{E_m} \rho_\uparrow(\epsilon)[\rho_\uparrow(E_m-\epsilon)+\rho_\downarrow(E_m-\epsilon)]d\epsilon. \quad (7)$$

Taking into account that the incident He($2\,^3S$) beam has nonunity polarization P_A, Eq. (7) must be rewritten to

$$N(E)_{a(p)} = \int_0^{E_m} \left(\frac{1+P}{2}\rho_{\uparrow(\downarrow)}(\epsilon) + \frac{1-P}{2}\rho_{\downarrow(\uparrow)}(\epsilon) \right) \times [\rho_{\uparrow(\downarrow)}(E_m-\epsilon)+\rho_{\downarrow(\uparrow)}(E_m-\epsilon)]d\epsilon, \quad (8)$$

where the degree of polarization P of the down(tunneling) electrons matches the polarization P_A of the incident He($2\,^3S$) beam and the up(ejected) electrons have no polarization other than that gained by a possible difference of spin densities $\rho_\uparrow$ and $\rho_\downarrow$.

After rearrangement of terms, Eq. (8) can finally be written in the symbolic form

$$N(E)_a = \frac{1+P}{2}(\rho_\uparrow * \rho_\uparrow)(E_m) + \frac{1-P}{2}(\rho_\downarrow * \rho_\downarrow)(E_m) + (\rho_\uparrow * \rho_\downarrow)(E_m), \quad (9)$$

$$N(E)_p = \frac{1+P}{2}(\rho_\downarrow * \rho_\downarrow)(E_m) + \frac{1-P}{2}(\rho_\uparrow * \rho_\uparrow)(E_m) + (\rho_\uparrow * \rho_\downarrow)(E_m), \quad (10)$$

where the symbol "$*$" denotes a Laplace convolution that is unique and reversible. So, in principle, the inversion of Eqs. (9) and (10) should deliver $\rho_\uparrow$ [$\rho_\downarrow$]. Difficulties arise from the fact that there are not only self-convolution terms in Eqs. (9), (10) but also a "coupling" term $(\rho_\uparrow * \rho_\downarrow)$. In addition, measured $N(E)$ are superposed by secondary electron background and noise.

Numerous attempts have been made (e.g., Refs. 1,25) on the numerical inversion of self-convolution processes in different types of electron spectroscopy. We extend the iterative algorithm of Dose and Fauster[26,27] on the treatment of spin polarization. Briefly, the strict equality of Eqs. (9), (10) is dropped in favor of the smoothest functions $N_p(E)$ [$N_a(E)$], which approximate maximally close to the measured discrete N_{p_i} and N_{a_i}. It turns out[27] that there is only one free parameter needed to control the contradicting requirements of smoothness and exactness of the fit. The value of the parameter is usually noncritical. We model $\rho_\uparrow$ [$\rho_\downarrow$] with cubic splines, which are the smoothest two times differentiable functions interpolating a given dataset.

We want to stress that this algorithm enables us to deconvolute our data without prior assumptions on the forms of $\rho_\uparrow$ and $\rho_\downarrow$ and to compute the confidence interval of the found functions which is determined by the error of the experimental data. It's important to note that the confidence interval allows us to test the reliability of the results and to draw definite conclusions concerning structures.

Deconvolution is done in two steps, first by unfolding the experimental data with the differential energy resolution function $\Delta E = f(E)$ of the detector to gain data with correct relative intensities, before the actual deconvolution is made. The function $\Delta E = f(E)$ was experimentally measured as well as numerically simulated for the spectrometer.

A strict test of our algorithm has been done by deconvolution and reconvolution of numerous test datasets. In addition to the treatment of our own experimental data, we tested the reliability of the results of our algorithm by comparing them with the data of Ferro *et al.*[11] on clean and oxygen covered Fe/Ag(001) which show similarity to our data on unannealed Fe/W(110). In Ref. 11, deconvolution starts with "guessed forms"[28] of $\rho_\uparrow$ and $\rho_\downarrow$, which are varied until satisfying consistence with experimental data is reached. The results are given in Fig. 2, which shows good agreement between our method and the method of Ref. 11. Further, we tested our method on a different system where structures at higher binding energies (5–8 eV) are present, namely clean cleaved GaAs(110), investigated by Pasquali *et al.*[29] This comparison is shown in Fig. 3 and demonstrates that structures are reproduced in the full energy range.

IV. RESULTS AND DISCUSSION

A. O/Fe/W(110)

Figures 4 and 5 show our measurements of the electron intensity (panel a) and asymmetry (panel b) as a function of the vacuum kinetic energy of the ejected electrons for unannealed (Fig. 4) and annealed (Fig. 5) Fe/W(110) films. Also (in panel c), the deconvoluted effective state densities $\rho_\uparrow$ and $\rho_\downarrow$ are shown.

For clean Fe films, the behavior at high kinetic energies near the Fermi level is attributed to $3d$ electrons. For these electrons a positive asymmetry is measured, which corresponds to a dominance of minority electrons in the surface vacuum region. The theoretical calculations[30] predict for bulklike Fe atoms a dominance of *majority*-spin states at the Fermi edge. These calculations show that the surface layer density of states (DOS) are narrowed due to the lower coordination number, with the result that the minority-spin contribution overwhelms the majority-spin at E_F for the surface layer. In the vacuum, minority-spin states become dominant especially in the region close to E_F.[30] This dominance is in agreement with our experimental results here and also with the measurements of the Onellion and co-workers group from Fe(110) on a GaAs substrate[4] and the Moroni and co-workers from Fe/Ag(100) (Refs. 11,17) and Fe/MgO(100).[12,17]

Spin-polarized UPS (SPUPS) studies of clean Fe/W(110) films[8] show bulklike behavior (majority dominance) at the Fermi energy and within an interval of about 1 eV below, independent of whether the excitation is done with HeI ($h\nu = 21.22$ eV) or with NeI ($h\nu = 16.85$ eV) radiation. This

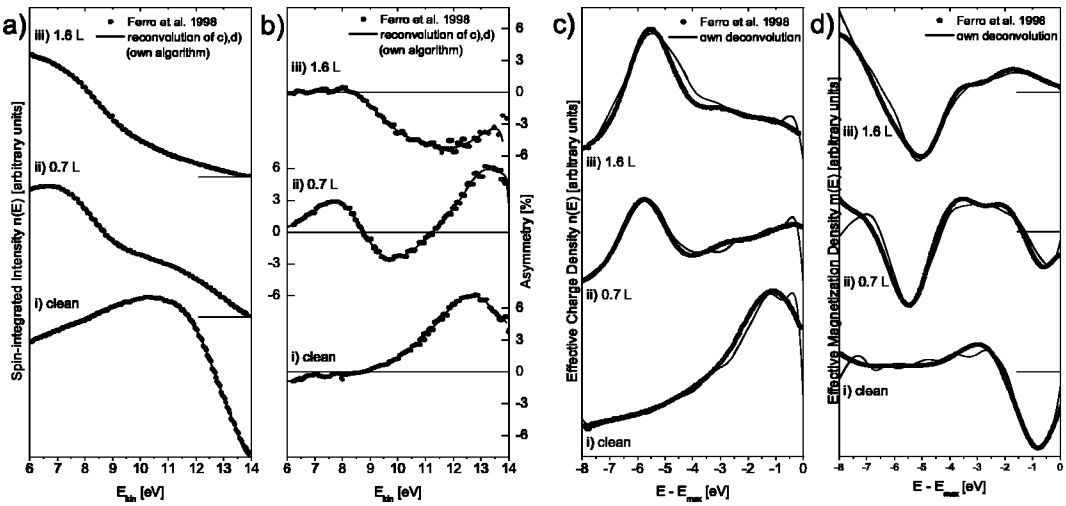

FIG. 2. Intensity (a) and asymmetry (b) of selected experimental data from Ferro *et al.* (Ref. 11). (i) clean Fe/Ag film, (ii) 0.7-L O_2, (iii) 1.6-L O_2 (1 L$=10^{-6}$ Torr s). Filled circles denotes data of Ferro *et al.*, solid lines are results of backconvolution of deconvoluted data gained by our method [see solid lines in (c) and (d)]. Note that Ferro *et al.* defines the asymmetry with opposite sign of Eq. (1). Further deconvoluted charge (c) and magnetization densities (d) of selected data from Ferro *et al.* (Ref. 11) by comparison. (i) clean Fe/Ag film, (ii) 0.7-L O_2, (iii) 1.6-L O_2 (1 L$=10^{-6}$ Torr s). Deconvolution results are given as "charge density" $n(E)=\rho_{\uparrow}+\rho_{\downarrow}$ ["magnetization density" $m(E)=\rho_{\uparrow}-\rho_{\downarrow}$]. Filled circles denotes deconvolution data of Ferro *et al.*, solid lines are results of our deconvolution.

behavior is in contrast to SPMDS findings. It is attributed to the different surface sensitivities of the two methods, with SPMDS probing the outermost region.

The size of the asymmetry maximum depends on the crystallographic quality of the prepared iron film. With annealed films we obtained 24%, whereas the unannealed films only showed about 15%. In Ref. 11, the maximum asymmetry is only 6% for Fe/Ag(100), annealed films on MgO show 9% (Ref. 12) [5%].[13]

We measured the asymmetry of the unannealed and annealed Fe/W(110) films as a function of oxygen exposure up to 80 L (1 L equals 10^{-6} Torr s), the results are shown in Fig. 4 (unannealed Fe) and Fig. 5 (annealed Fe), for earlier published results see Refs. 8,31. With oxygen exposure significant changes are observed. At an exposure of about 1–2 L a structure occurs with a positive asymmetry with a maximum at about 5.5 eV kinetic energy. This structure can be assigned to O_{2p} states,[32] also found in SPUPS.[10] With further exposure the oxygen structure decreases, which may be interpreted that the chemisorbed oxygen has been partially transformed to nonferromagnetic iron oxide.

Figure 6 shows a comparison of UPS measurements[10] and our deconvoluted MDS data from Fig. 5. As found by angle-resolved x-ray photoemission spectroscopic (XPS) measurements,[33] the oxygen structure consists of the p_x level at the low-energy side and the p_z level at the high-energy side. In MDS, similar to UPS,[10] these levels are broad and cannot be separated. The analysis of this structure by our deconvolution method provides the seize of the energy splitting (exchange splitting) between the majority and minority O_{2p} bands which is shown in Fig. 7 together with SPUPS results[10] for comparison. The exchange splitting decreases with higher oxygen exposure and is also dependent on surface order where the annealed films show generally higher

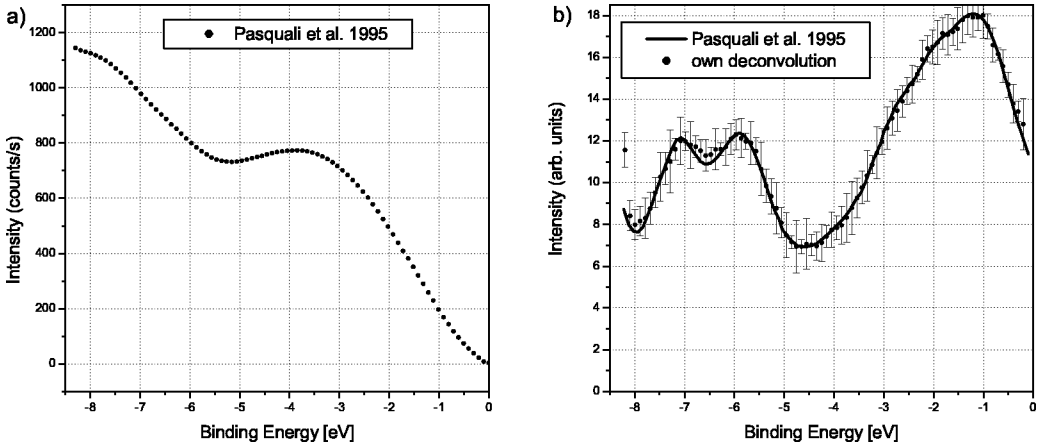

FIG. 3. (a) MD spectrum of clean cleaved GaAs(110) (Ref. 29). (b) Deconvolution of MD spectrum (solid line) (Ref. 29) compared with our deconvolution results (filled circles with error bars indicating confidence intervals).

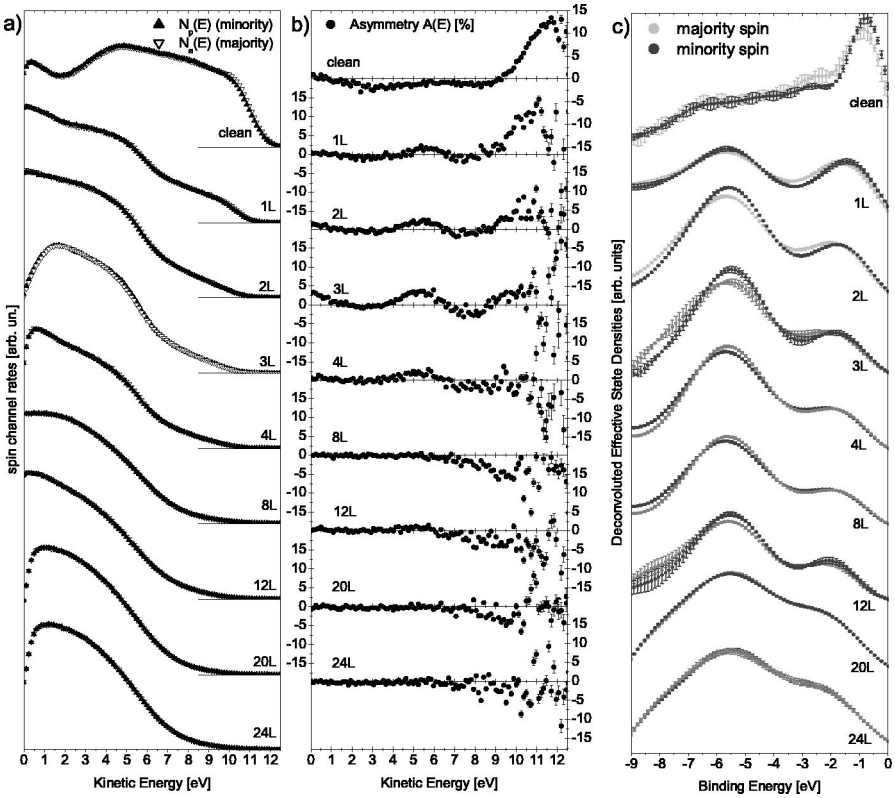

FIG. 4. Spin channel rates (a), asymmetry (b), and deconvoluted state densities (c) for different oxygen exposure on unannealed Fe(110).

splittings. This is in agreement with the data on Fe/Ag(100) (Refs. 11,17) (unannealed film) and Fe/MgO(100) (annealed film).[12,17]

From about 2-L to 4-L oxygen exposure, the asymmetry for electrons near the Fermi edge changes sign. This depends on surface order and occurs for unannealed films at about 3 L. The annealed films show negative asymmetry only in a region up to 1.5 eV below E_F (Fig. 5), whereas unannealed films have this region extended up to 5.5 eV below E_F (Fig. 4). The change of sign is in agreement with measurements

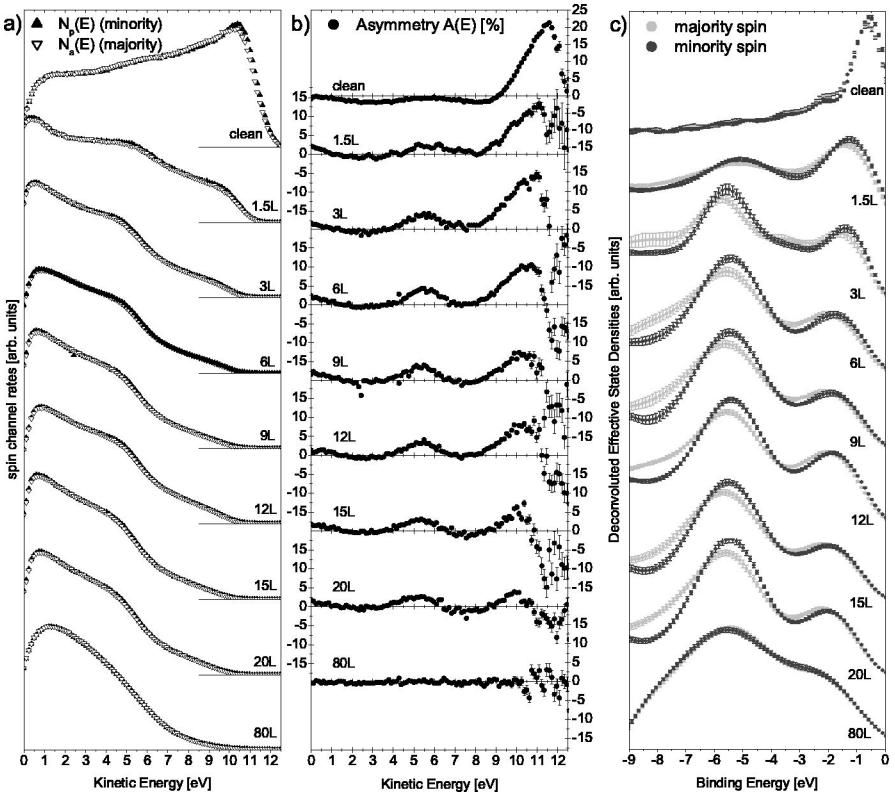

FIG. 5. Spin channel rates (a), asymmetry (b), and deconvoluted state densities (c) for different oxygen exposure on annealed Fe(110).

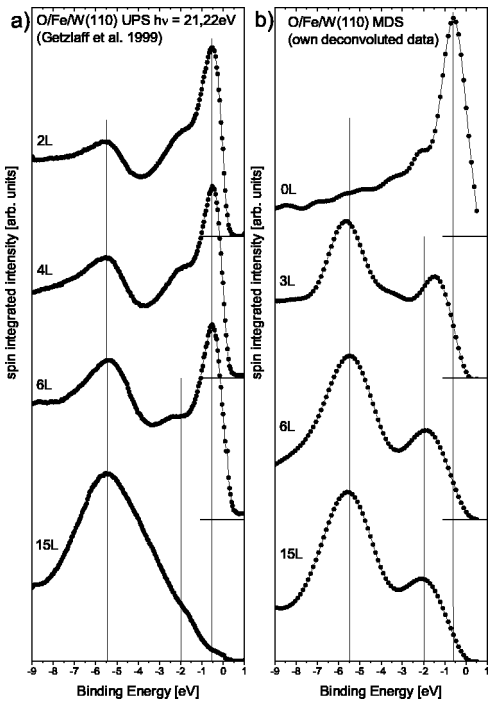

FIG. 6. Spin integrated intensities for different oxygen exposure on (a) annealed Fe measured with UPS (extracted from Ref. 10) and (b) MDS (own data).

performed on O/Fe(110)/GaAs,[4] O/Fe/Ag(001),[11,17] O/Fe/MgO(001),[12,13,17] and also with a theoretical calculation[20] that predicts a dominance of majority electrons in the surface vacuum region of O/Fe(110). It should be noted that this calculation is based on a $p(1\times1)$ structure of the oxygen, whereas the experimentally obtained $c(2\times2)$ and $c(3\times1)$ structures are present.[14,34] As can be seen in Fig. 5(c) the change of sign is associated with the decrease of the substrate Fe_{3d} feature at ~-0.6 eV binding energy and the rise of a structure at ~-2 eV binding energy that can be attributed to Fe_{3d} emissions of the forming iron oxide. Also the Fe core levels show a oxygen-induced shift in binding energy, as can be seen by means of XPS and magnetic linear dichroism.[35] In SPUPS measurements,[10] the structure at ~-2 eV binding energy is only vaguely visible (see Fig. 6 for comparison). At very high oxygen exposures (>600 L) FeO transforms to Fe_3O_4, which forms a magnetic bilayer with the substrate, so that this structure shows an asymmetry in SPUPS.[35]

With further increasing the coverage, the overall asymmetry decreases and is finally reduced to zero, pointing to a complete transformation of the surface to iron oxide and, as a consequence of this, the forming of a magnetic dead zone (in the outermost region of the surface). Comparing Figs. 4 and 5, we note that this occurs for the annealed films at higher oxygen exposures indicating a lower reactivity of the ordered surface.

B. O/Co/W(110)

The measured intensities and asymmetries as a function of oxygen exposure for Co(0001)/W(110) are shown in Fig. 8,

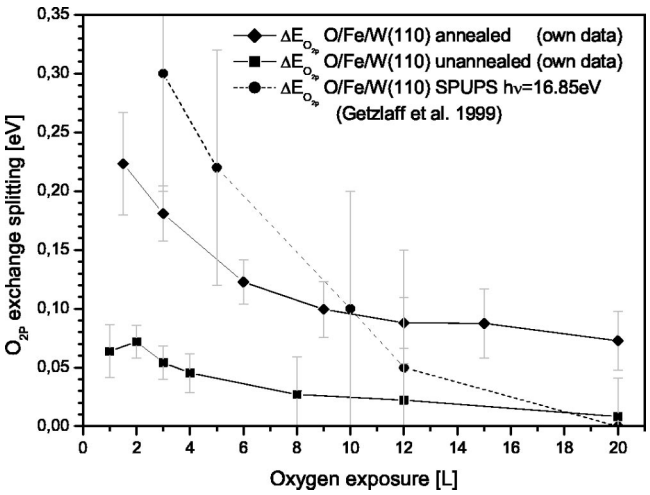

FIG. 7. Exchange splitting of O_{2p} derived states for different oxygen exposure on unannealed and annealed Fe(110).

for earlier published results see Ref. 8. There is a theoretical calculation of the surface-layer-projected spin density of states for uncovered Co(0001) available.[36] This calculation predicts a dominance of minority-spin electrons near the Fermi energy. The measured positive yield asymmetry agrees with that. The maximum achieved asymmetry is 15%, independent of further annealing. This may be attributed to layer by layer growth of Co on W(110) below 450 K.[37] Compared to clean Fe/W(110), the Co_{3d} feature in the deconvoluted state densities [Fig. 8(c)] is much broader, also in comparison to SPUPS measurements on Co(0001) (Fig. 9).[38] This is attributed to dispersion effects, as Co(0001) shows dispersing minority bands near the Fermi edge. In UPS measurements,[7] this leads to significant differences in the photoelectron spectra measured at different emission angles ($k_{\|}$ dispersion).

For oxygen covered Co(0001) there is, as far as we know, no surface-layer-projected spin-density calculation in the literature. But for a bcc-Co(110) five-layer slab, covered with one-layer oxygen, a calculation exists.[39] This calculation shows that at the Fermi edge the dominance of the minority-spin electrons in the oxygen layer remains the same as in the Co substrate. This agrees with our measurement. The oxygen-induced structure at about 5.5 eV is also present here. The asymmetry increases at this kinetic energy from zero up to 5% and remains constant up to an exposure of 24 L. This reflects the lower chemical reactivity of oxygen with the cobalt film than with iron. In the structure near the Fermi energy, the asymmetry decreases slowly with increasing exposure *without changing sign*. This behavior is markedly different from that for iron. The SPUPS studies of clean and oxygen-covered Co(0001) film showed[38] that more majority electrons are emitted in an energy interval of about 1 eV at the Fermi edge after excitation with NeI ($h\nu=16.85$ eV) and ArI ($h\nu=11.83$ eV) light, but more minority electrons are emitted using HeI light. This behavior is different to our SPMDS findings and shows the different surface sensitivity of the two methods.

The oxygen-induced binding-energy shift of the substrate $3d$ feature is also present here [see Figs. 8(c) and 9]. Oxygen

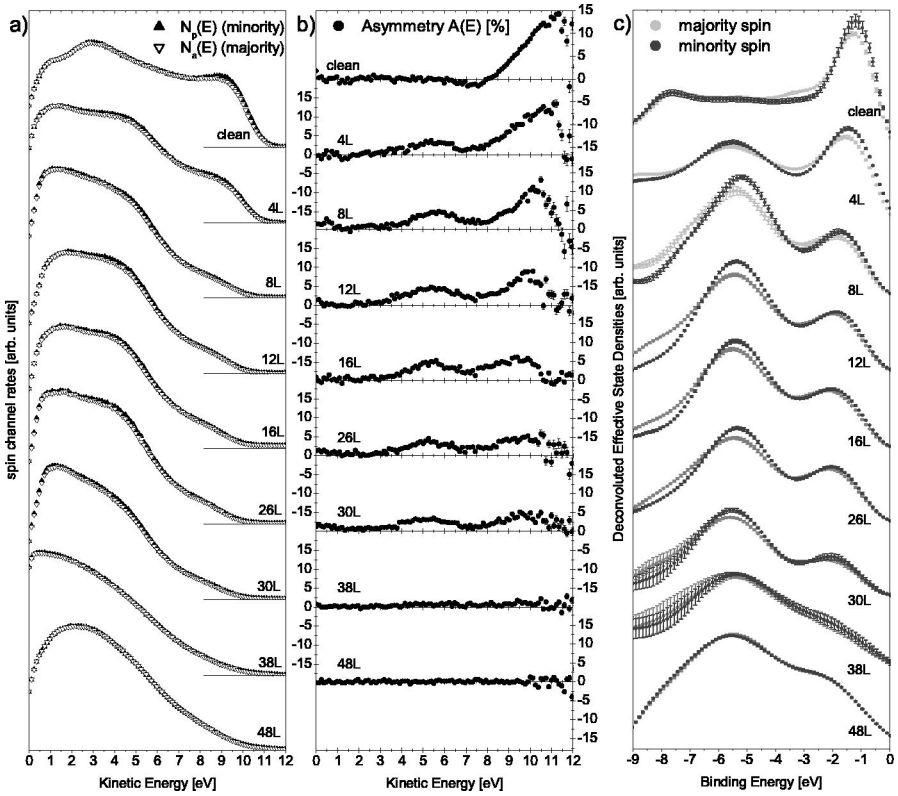

FIG. 8. Spin channel rates (a), asymmetry (b), and deconvoluted state densities (c) for different oxygen exposure on Co(0001).

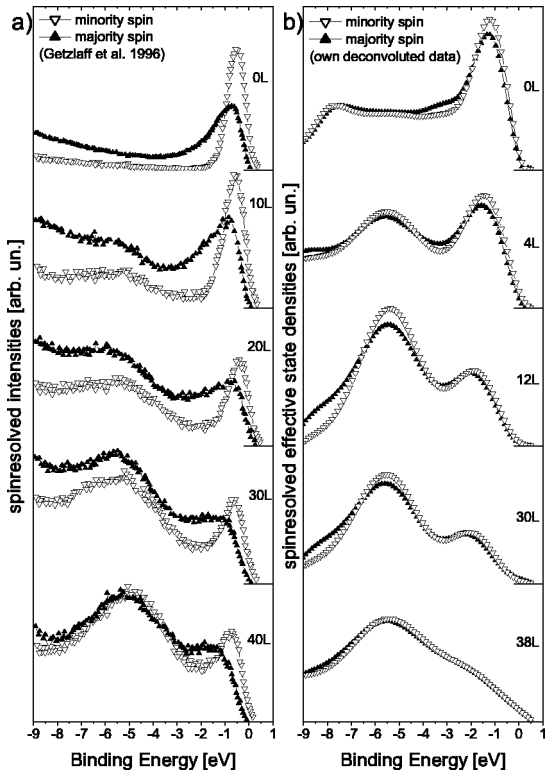

FIG. 9. Spin resolved intensities for different oxygen exposure on Co(0001) measured with UPS (extracted from Ref. 38) and MDS (own deconvoluted data).

on Co, like on Fe, shows an exchange splitting in the O_{2p}-derived surface states (see Fig. 10).

V. SUMMARY

By means of SPMDS, we have determined magnetic and electronic properties of chemisorbed oxygen overlayers on magnetized Fe(110) and Co(0001) films. A recently developed algorithm allows us to deconvolute our data thereby revealing the surface state densities effective in MDS. The algorithm enables us to deconvolute the data without making any prior assumptions on the form of results and in addition

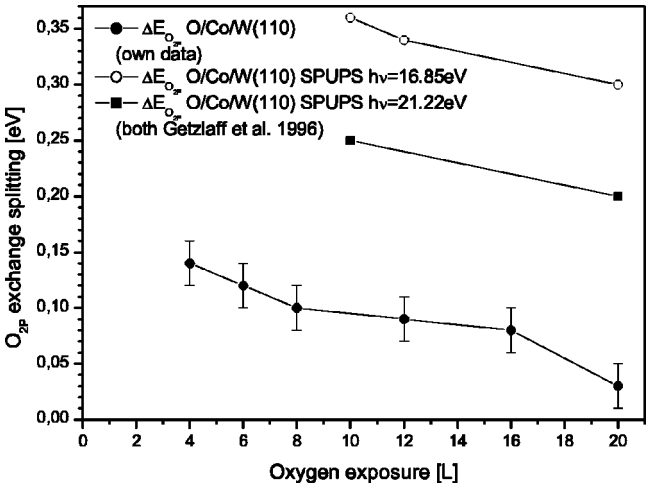

FIG. 10. Exchange splitting of O_{2p}-derived states for different oxygen exposure on Co(0001). MDS (own deconvoluted data) and UPS (extracted from Ref. 38) measurements in comparison.

to determine the confidence interval. This provides an opportunity of direct comparison with the state density information gained by other surface spectroscopic methods (SPUPS, AES, MCD, etc.).

Low oxygen exposure leads to atomically bonded, chemisorbed oxygen as can be seen by the occurrence of O_2p-derived bands and their detected exchange splitting. This reflects a magnetic coupling between the chemisorbed oxygen and the magnetized film. For higher exposures, formation of nonmagnetic oxides was observed resulting in vanishing asymmetry of majority and minority state components. The magnitude of exchange splitting depends on surface order. Higher-ordered (annealed) films show higher exchange splittings, indicating a stronger magnetic coupling. Contrary to SPUPS findings, Fe films show a change of sign in the asymmetry right below E_F with oxygen exposure above 3 L, confirming a theoretically predicted dominance of majority electrons in the surface vacuum region of O/Fe(110). This shows the specific sensitivity of MDS in the outermost region of the surface.

[1] W. Sesselmann, B. Woratscheck, J. Küppers, G. Ertl, and H. Haberland, Phys. Rev. B **35**, 1547 (1987).
[2] H. Morgner, Adv. At., Mol., Opt. Phys. (Academic Press, New York, 1999), Vol. 42B, pp. 387–488.
[3] Y. Harada, S. Masuda, and H. Ozaki, Chem. Rev. **97**, 1897 (1997).
[4] M. Onellion, M.W. Hart, F.B. Dunning, and G.K. Walters, Phys. Rev. Lett. **52**, 380 (1984).
[5] M.S. Hammond, F.B. Dunning, G.K. Walters, and G.A. Prinz, Phys. Rev. B **45**, 3674 (1992).
[6] D.E. Eastman and J.L. Freeouf, Phys. Rev. Lett. **34**, 395 (1975).
[7] M. Getzlaff, J. Bansmann, J. Braun, and G. Schönhense, J. Magn. Magn. Mater. **161**, 70 (1996).
[8] M. Getzlaff, D. Egert, P. Rappolt, M. Wilhelm, H. Steidl, G. Baum, and W. Raith, Surf. Sci. **331-333**, 1404 (1995).
[9] M. Salvietti, R. Moroni, M. Canepa, and L. Mattera, J. Electron Spectrosc. Relat. Phenom. **76**, 677 (1995).
[10] M. Getzlaff, J. Bansmann, and G. Schönhense, J. Magn. Magn. Mater. **192**, 458 (1999).
[11] P. Ferro, R. Moroni, M. Salvietti, M. Canepa, and L. Mattera, Surf. Sci. **407**, 212 (1998).
[12] R. Moroni, F. Bisio, M. Canepa, and L. Mattera, Appl. Surf. Sci. **175-176**, 797 (2001).
[13] Y. Yamauchi and M. Kurahashi, Appl. Surf. Sci. **169-170**, 236 (2001).
[14] A. Hodgson, A. Wight, and G. Worthy, Surf. Sci. **319**, 119 (1994).
[15] M.E. Bridge and R.M. Lambert, Surf. Sci. **82**, 413 (1979).
[16] G.R. Castro and J. Küppers, Surf. Sci. **123**, 456 (1982).
[17] R. Moroni, F. Bisio, M. Canepa, and L. Mattera, Surf. Sci. **433-435**, 676 (1999).
[18] G. Baum, W. Raith, and H. Steidl, Z. Phys. D: At., Mol. Clusters **10**, 171 (1988).
[19] H. Steidl and G. Baum, *Selected Topics on Electron Physics* (Plenum Press, New York, 1996), pp. 233–241.
[20] D.R. Penn and P. Apell, Phys. Rev. B **41**, 3303 (1990).
[21] L.A. Salmi, Phys. Rev. B **46**, 4180 (1992).
[22] H.D. Hagstrum and G.E. Becker, Phys. Rev. B **4**, 4187 (1971).
[23] E. Hood, F. Bozso, and H. Metiu, Surf. Sci. **161**, 491 (1985).
[24] H. D. Hagstrum, *Electron and Ion Spectroscopy of Solids* (Plenum Press, New York, 1978), p. 273.
[25] C. Boiziau, C. Garot, R. Nuvolone, and R. Roussel, Surf. Sci. **91**, 313 (1980).
[26] V. Dose and T. Fauster, Appl. Phys. **20**, 299 (1979).
[27] V. Dose, T. Fauster, and H.-J. Gossmann, J. Comput. Phys. **41**, 34 (1981).
[28] M. Salvietti, R. Moroni, P. Ferro, M. Canepa, and L. Mattera, Phys. Rev. B **54**, 14 758 (1996).
[29] L. Pasquali, S. Nannarone, M. Canepa, and L. Mattera, Phys. Rev. B **52**, 17 335 (1995).
[30] R. Wu and A.J. Freeman, Phys. Rev. Lett. **69**, 2867 (1992).
[31] M. Getzlaff, D. Egert, P. Rappolt, M. Wilhelm, H. Steidl, G. Baum, and W. Raith, J. Magn. Magn. Mater. **140-144**, 727 (1995).
[32] M. Getzlaff, J. Bansmann, C. Westphal, and G. Schönhense, J. Magn. Magn. Mater. **104-107**, 1781 (1992).
[33] Y. Sakisaka, T. Komeda, T. Miyano, M. Onchi, S. Masuda, Y. Harada, K. Yagi, and H. Kato, Surf. Sci. **164**, 220 (1985).
[34] H.-J. Kim and E. Vescovo, Phys. Rev. B **58**, 14 047 (1998).
[35] H.-J. Kim, J.-H. Park, and E. Vescovo, Phys. Rev. B **61**, 15 288 (2000).
[36] R. Wu, D.S. Wang, and A.J. Freeman, J. Magn. Magn. Mater. **132**, 103 (1994).
[37] B.G. Johnsonn, P.J. Berlowitz, D.W. Goodman, and C.H. Bartholemew, Surf. Sci. **217**, 13 (1989).
[38] M. Getzlaff, J. Bansmann, and G. Schönhense, J. Electron Spectrosc. Relat. Phenom. **77**, 197 (1996).
[39] B. Weimert, Ph.D. thesis, Technical University Clausthal-Zellerfeld, 1995.